Analytica Chimica Acta 875 (2015) 22–32

Contents lists available at ScienceDirect

Analytica Chimica Acta

journal homepage: www.elsevier.com/locate/aca

Thermally induced solid-state transformation of cimetidine. A multi-spectroscopic/chemometrics determination of the kinetics of the process and structural elucidation of one of the products as a stable N_3-enamino tautomer

Natalia L. Calvo, Sebastian O. Simonetti, Rubén M. Maggio, Teodoro S. Kaufman *

Pharmaceutical Analysis, Department of Organic Chemistry, School of Pharmaceutical and Biochemical Sciences, National University of Rosario and Institute of Chemistry of Rosario (IQUIR, CONICET-UNR), Suipacha 531, Rosario (S2002LRK), Argentina

HIGHLIGHTS

- Thermally stressed cimetidine above its melting point affords a stable N_3 tautomer.
- Multi-spectroscopic/chemometric approach developed to monitor tautomerization.
- First combined use of NMR, UV and IR spectroscopies with chemometrics.
- Solid cimetidine suffers first order degradation upon submission to dry heat.
- Theoretical chemistry analysis confirmed the relative stability of cimetidine tautomer.

GRAPHICAL ABSTRACT

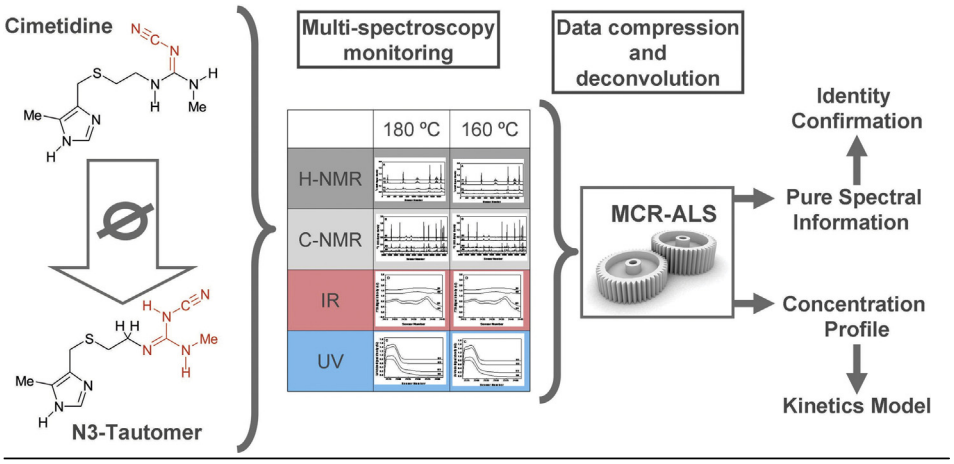

ARTICLE INFO

Article history:
Received 10 October 2014
Received in revised form 2 February 2015
Accepted 10 February 2015
Available online 12 February 2015

Keywords:
Cimetidine
Stable tautomeric form
Multivariate curve resolution with alternating least squares determination
Multi-spectroscopic/chemometric approach
Spectroscopic characterization
Nuclear magnetic resonance spectroscopy

ABSTRACT

Exposure of cimetidine (CIM) to dry heat (160–180 °C) afforded, upon cooling, a glassy solid containing new and hitherto unknown products. The kinetics of this process was studied by a second order chemometrics-assisted multi-spectroscopic approach. Proton and carbon-13 nuclear magnetic resonance (NMR), as well as ultraviolet and infrared spectroscopic data were jointly used, whereas multivariate curve resolution with alternating least squares (MCR-ALS) was employed as the chemometrics method to extract process information. It was established that drug degradation follows a first order kinetics.

One of the products was structurally characterized by mono- and bi-dimensional NMR experiments. It was found to be the N_3-enamino tautomer (TAU) of CIM, resulting from the thermal isomerization of the double bond of the cyanoguanidine moiety of the drug, from the imine form to its N_3-enamine state.

The thus generated tautomer demonstrated to be stable for months in the glassy solid and in methanolic solutions. A theoretical study of CIM and TAU revealed that the latter is less stable; however,

* Corresponding author. Tel.: +54 341 4370477x118; fax: +54 341 4370477x112.
E-mail address: kaufman@iquir-conicet.gov.ar (T.S. Kaufman).

http://dx.doi.org/10.1016/j.aca.2015.02.033

the energy barrier for tautomer interconversion is high enough, precluding the process to proceed rapidly at room temperature.

1. Introduction

The detection and identification of impurities structurally related to drug substances is of utmost importance in the modern pharmaceutical industry. Limitation of these impurities constitutes an increasingly complex science-based requirement [1]. Recognized regulatory bodies (ICH [2,3], FDA, EUDRA) and many pharmacopeias [4] emphasize on this topic, setting maximum levels to determined, undetermined and total impurities.

These impurities may come from the manufacturing process, but can also be developed during manipulation of the active pharmaceutical ingredient (API), including the formulation and storage stages in bulk and formulated products. These multiple scenarios complicate research toward the detection and elucidation of new pharmaceutical impurities, while enhancing the relevance of this endeavor.

Tautomers are a kind of constitutional isomers that coexist in equilibrium and are more or less readily interconvertible. Prototropic tautomerism refers to the addition of a proton at one molecular site with its concomitant removal from another place. Tautomer interconversion takes place in response to media changes, such as variation of pH, dipolar moment and hydrogen bonding ability; it may also occur when the crystalline structure is lost, such as in case of melting and dissolution of a compound.

The stability of tautomers is widely variable; therefore, it is difficult to predict the possibility of being separated, isolated or analyzed. It has been suggested that when the major form of an API is the more thermodynamically stable tautomer, any other tautomer should be considered an impurity ('tautomer of the API'), because stable tautomers may have a different pharmacological activity [5].

In spite the phenomenon of tautomerism is a subject of intense research and despite the fact that many known drugs exhibit tautomerism [6], there has been relatively scarce literature relating to the preparation or characterization of tautomeric impurities from the final APIs [5,7,8].

Cimetidine (CIM) is *N*″-cyano-*N*-methyl-*N*′-[2-[[(5-methyl-1*H*-imidazol-4-yl)methyl]thio]-ethyl]-guanidine. This heterocycle, which became the first blockbuster drug, is a histamine analogue, in which the imidazole ring is substituted by a methyl group and a side chain which is extended through a thioether bond, and ends in a cyanoguanidine moiety (Fig. 1). CIM acts as an antagonist of the type 2 histamine receptors (H2R) located on the surface of stomach parietal cells. The drug inhibits acid secretion induced by histamine, gastrin or pentagastrin, accelerating the healing of gastrointestinal ulcers [9,10].

Thus, despite the availability of other alternatives, CIM is still widely prescribed as an anti-ulcer agent. CIM seems to have additional desirable properties related to cancer [11–13], modulation of the immune response [14] and skin [15] therapeutics.

CIM exhibits a rich structural polymorphism, with at least four reproducible crystalline forms (A–D) and a monohydrate (M1). The drug is also an extraordinary example of isomerism. The imidazole ring in the structure of CIM may give rise to a pair of tautomers (**X** and **Y**,Fig. 1), depending on which nitrogen atom of the heterocycle (N_2 or N_1) is attached to hydrogen (atom numbering as in ref. [21]). However, only the more stable N_1—H form (**X**) has been observed in the crystal states [16–18] and in M1, and rationalized through theoretical calculations [19].

In addition, the trisubstituted guanidine moiety may exhibit both, geometric isomerism (*syn–anti*) and three imine–enamine type (with regards to the nitrogen carrying the cyano moiety) non-equivalent tautomers, which may take place independently, to yield six possible alternatives (**1–6**) [20]. According to X-ray crystal data, polymorphic forms C, D and M1 are different packings of the N_1—H *anti* imine isomer (**X1**), while form A is a N_1—H *syn* imine isomer (**X4**) [21,22]. This is possible because the barrier to rotation about a C=N bond is smaller than that about a C=C bond, and decreases with the electronegativity of the substituents on the nitrogen atom.

Regarding the impurities of CIM, in addition to those resulting from the manufacturing process [23], it has been reported that the drug may undergo degradation through hydrolysis and oxidation [24–26]. The group of Evans disclosed the sulfur-specific detection of impurities in cimetidine drug substance using liquid chromatography coupled to high resolution inductively coupled plasma mass spectrometry (LC/HR-ICP-MS) and electrospray mass spectrometry (ESI-MS) [27].

Bauer-Brandl informed that CIM undergoes polymorphic transformations in the dry state upon milling during long periods of time, which include substantial amorphization [28]. Amorphous forms of CIM have also been obtained by heating the drug at 150 °C and pouring the melt on liquid nitrogen, and by processing pre-compressed granules of the drug in a candy cotton machine at 150 °C [29]. Interestingly, the 200 MHz NMR spectra of these products in acetone-d_6 demonstrated that no impurities were formed during the conditions of this amorphization process.

CIM melts slightly above 140 °C. In the course of our studies on the crystal forms of CIM [30],we were puzzled about the inability of the vitreous form to revert to a crystalline phase, when prepared by heating CIM up to approximately 160 °C [29]. The same phenomenon was reported earlier by other researchers which, employing thermal methods and polarized light thermal microscopy, found no evidence

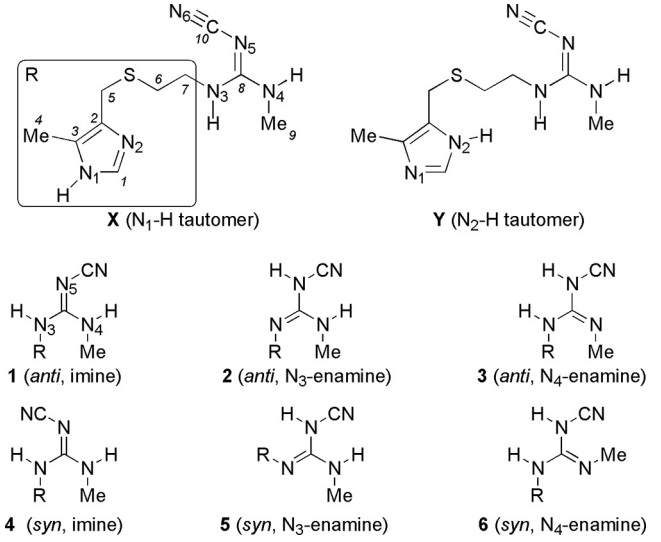

Fig. 1. The different possible geometric isomers and tautomers of cimetidine. Form A is a N_1—H *syn* imine isomer (**X4**). Forms C, D and M1 are different packings of the N_1—H *anti* imine isomer (**X1**).

of a crystalline transition related to recrystallization during the cooling process [31,32].

In addition, it was observed that CIM exhibits high thermal stability and published thermogravimetric data confirm that CIM does not lose weight upon heating up to 190 °C [31,33,34]. Therefore, all these experiments suggested that an irreversible thermal process was taking place during heating and cooling.

Considering the known ability of the substituted guanidines to undergo tautomeric interconversions [35], we decided to examine the composition of melted CIM. Therefore, herein we disclose the thermally-promoted generation of a stable tautomer (TAU) of the drug, a multispectroscopic chemometrics-assisted study of the kinetics of its generation, the exhaustive characterization of TAU, jointly employing various NMR experiments and a theoretical study to explain its unexpected stability. NMR is a powerful and highly structure-sensitive spectroscopy, useful in pharmaceutical analysis of impurities [36]; coupling of NMR to chemometrics methodologies in order to gain knowledge about dynamic systems was reported in comparatively few cases [37,38].

2. Experimental

2.1. Chemicals

Cimetidine (polymorph A), bulk drug of pharmaceutical-grade (BP 2002), was acquired to Saporiti (Buenos Aires, Argentina). During the experiments, the drug was kept in a desiccator, protected from light. MeOH-d_4 (99.8% atom-d) was acquired from Cambridge Isotope Labs, Inc. (Andover, MA, USA); all other solvents were of analytical grade and were used as received.

2.2. Instrumentation

Controlled thermal heating for the preparation of TAU was carried out with a Talboys fully digital hotplate-stirrer (Troemner, Thorofare, USA) fit with an RTD temperature probe immersed in the silicon oil bath containing the samples, capable of controlling the bath temperature to ±1 °C of the pre-set level.

Optical microscopy was carried out with the aid of an Ernst Leitz Wetzlar model 350 hot-stage polarized light microscope. Melted samples were visualized with a 5.0 Megapixels Beion CMOS digital camera [Shanghai Beion Medical Technology Co., Ltd., Shangai, China; resolution 2592 × 1944 ($H \times V$)].

FTIR spectra (20 scans each) were acquired in a Shimadzu Prestige 21 spectrometer (Shimadzu Corp., Kyoto, Japan), in the absorbance mode, over a wavenumber range of 4000–600 cm^{-1} and at a resolution of 4 cm^{-1}. The ATR experiments were carried out with a diamond-based ATR accessory (GladiATR, Pike Technologies, Madison, USA), fitted with a Pike temperature control unit.

The spectroscopic determinations in the UV were carried out with an Agilent 8453 UV–DAD spectrophotometer (Agilent Technologies, Santa Clara, USA), controlled by the Chemstation v.B04-02 software, at a 1 nm resolution, between 200 and 400 nm. The determinations were performed in a quartz cuvette (10 mm optical path length) against a blank of MeOH.

The ^1H and ^{13}C NMR spectra were acquired in MeOH-d_4 in a Bruker Avance spectrometer (300.13 and 75.48 MHz for ^1H and ^{13}C, respectively) with tetramethylsilane (TMS) as internal standard (Bruker BioSpin GmbH, Karlsruhe, Germany). The ^1H and ^{13}C NMR spectra were exported in txt format.

NMR signals are abbreviated as follows: s = singlet; d = doublet; b = broad signal. The chemical shifts (δ) are reported in ppm downfield from TMS; coupling constants (J) and widths of wide signals at half peak heights ($w_{1/2}$) are expressed in Hz. Special 1D (DEPT 135, NOE and TOCSY) and 2D (COSY, HMBC and HSQC) NMR experiments were also acquired, to better ascertain H—H and C—H connectivity and proximity. The corresponding pulse programs were taken from the Bruker software library.

2.3. Thermally-assisted generation of TAU

Accurately weighed amounts of CIM (30.0 mg) were quantitatively transferred to a series of 5 mm oven-dried NMR tubes previously flushed with nitrogen. The so prepared tubes were flushed again with nitrogen before being tightly capped. The tubes were then immersed in a magnetically stirred silicon bath, preheated to the desired temperature (160 °C or 180 °C). The samples were exposed to these conditions for pre-established times, when they were removed from the bath and left to attain room temperature.

2.4. Preparation of the samples for spectroscopic studies

For NMR spectroscopy: the heat-treated samples were dissolved with 0.480 mL of MeOH-d_4. The samples were kept in at 4 °C until use.

For UV and FTIR spectroscopy: the samples prepared for NMR spectroscopy were quantitatively transferred to 1 mL volumetric flasks and diluted to the corresponding marks with MeOH, to yield 30 mg mL^{-1} solutions.

For FTIR studies, 50 μL of each sample (approximately 1.5 mg) was carefully deposited on the ATR crystal. The solvent was left to evaporate before each determination. Data acquisition was carried out at 75 °C.

For UV studies, a 0.200 mL aliquot of the samples was transferred to a 10 mL volumetric flask and diluted to the mark with MeOH. A known volume (0.200 mL) of the resulting solution was diluted again with MeOH to 10 mL, in a volumetric flask, yielding final solutions containing a combined amount of 12 μg mL^{-1} of the analytes.

2.5. Chemometrics and graphics software

The ^1H and ^{13}C NMR data were processed with Topspin v. 2.0 (Bruker) and converted to ASCII files employing the 'convbin2asc' routine.

Multivariate curve resolution with alternating least squares (MCR-ALS) was employed for the chemometrics computations [39]. The computer routines involving spectral data manipulation and the MCR-ALS method were run in Matlab R2010a (Mathworks, Natick, USA). Spectra were aligned employing the correlation optimized warping (COW) algorithm [40], and polished by removing the non-informative regions. Kinetics estimations, statistical data analyses and miscellaneous graphics were performed using Origin 8.5 (OriginLab Co., Northampton, USA).

2.6. Theoretical (quantum mechanics) calculations

The theoretical ab initio Hartree–Fock and B3LYP density functional hybrid method calculations were carried out on a personal computer fitted with an Intel Core I5 microprocessor, employing the Gaussian 09 program package [41], on structures of the compounds drawn using Gaussview 5.08 (Gaussian, Inc., Wallingford, CT, 2009).

The geometries of CIM and TAU were determined, and the transition state (TS) was located and optimized at the level of restricted Hartree–Fock (RHF) and density functional theory (B3LYP), using the 6-31 + G(D) basis set. All structures were completely optimized without any symmetry restrictions. For all systems studied, vibrational frequency calculations were carried out to confirm that they converged to true minima. The conformers

were defined as true minima by diagonalization of their Hessian (force constant) matrices at the same level and making sure that all frequencies are real. Optimized geometries from the RHF level were taken as initial geometries to minimize at the B3LYP level. In general, the fully optimized geometries from prior calculations were used as starting points for calculations using the higher-level (B3LYP/3-21 + G* and B3LYP/6-311 + G**) basis sets.

The geometries of the true local minima of the potential energy surface were confirmed by positive values of all the calculated vibrational wave numbers. The stationary structures were confirmed by ascertaining that all ground states have only real frequencies.

2.7. Spectral polishing and data pre-treatment

NMR (^{1}H and ^{13}C), UV–vis and FTIR data were acquired from each sample. The experiments at 160 °C and 180 °C resulted in 5 and 7 spectra, respectively. The informative regions were extracted from the corresponding spectral matrices.

For ^{1}H NMR: the polished data matrix was built by joining the most informative regions, corresponding to the following chemical shift intervals: 7.6346–7.4166, 4.0278–3.2153, 2.9775–2.7793, 2.7674–2.5534 and 2.2640–2.1253 ppm. Data were submitted to peak alignment and normalization, employing the signal of residual MeOH (δ 3.3280) as reference and the total number of sensors was halved by removing the even sensors, affording final matrices with 1998 sensors per sample.

For ^{13}C NMR: the polished data matrix included the following shielding intervals: 166.56–161.46, 139.22–118.81, 60.86–59.77, 42.63–41.69, 35.71–28.05, 27.54–26.96 and 10.56–8.01. Data were subjected to the same alignment and normalization process of ^{1}H NMR data, yielding two final matrices with 5267 sensors per spectrum.

For the UV–vis spectra: the spectral range was the 200–348 nm region, totaling 149 sensors per sample; data were processed with no additional treatments.

For the FTIR spectra: the spectra were normalized relative to the 713.6 cm^{-1} signal, taken as reference. The selected informative region was that between 771.5 and 829.4 cm^{-1} (31 sensors $sample^{-1}$).

2.8. ^{1}H and ^{13}C spectral data of CIM and TAU

Data of CIM: ^{1}H NMR (300 MHz, δ): 2.21 (s, 3H, H-4), 2.79 (s, 3H, H-9), 2.60 (dd, 2H, J = 7.1 Hz, H-6), 3.70 (s, 2H, H-5), 3.35 (dd, 2H, J = 7.1 Hz, H-7), 4.95 (bs, 3H, $w_{1/2}$ = 4.5 Hz, 3 × NH) and 7.48 (s, 1H, H-1); ^{13}C NMR (75 MHz, δ): 10.1 (C-4), 27.3 (C-5), 28.7 (C-9), 31.6 (C-6), 42.1 (C-7), 127.7 (C-3), 120.1 (C-10), 134.7 (C-1), 130.7 (C-2) and 161.9 (C-8).

Data of TAU: ^{1}H NMR (300 MHz, δ): 2.18 (s, 3H, H-4), 2.81 (s, 3H, H-9), 3.28 (dd, 2H, J = 7.4 Hz, H-6), 3.64 (s, 2H, H-5), 3.89 (dd, 2H, J = 7.4 Hz, H-7), 4.95 (bs, 3H, $w_{1/2}$ = 4.5 Hz, 3 × NH) and 7.54 (s, 1H, H-1); ^{13}C NMR (75 MHz, δ): 8.7 (C-4), 31.0 (C-9), 28.4 (C-5), 35.5 (C-6), 60.4 (C-7), 126.0 (C-3), 126.1 (C-10), 135.1 (C-1), 130.5 (C-2) and 166.1 (C-8).

2.9. Theoretical background of MCR-ALS [39,42]

The following notation was chosen to write the matrix equations: scalars are represented by bold lowercase letters, matrices are designed by bold uppercase letters and the superscript "T" means the transposed matrix.

According to this matrix notation, the multi-wavelength extension of Lambert–Beer's law can be expressed as in Eq. (1),

$$\mathbf{D} = \mathbf{C}\mathbf{S}^{\mathrm{T}} + \mathbf{E} \quad (1)$$

where the rows of matrix **D** are the spectra measured during a single experiment, the columns of matrix **C** are associated with the concentration profiles and the columns of matrix **S** are the corresponding pure spectra of the involved species. **E** is the matrix of error associated to model fitting or the instrumental noise.

The goal of MCR-ALS is to perform the bilinear decomposition of the input data matrix **D** into the actual or true pure response profiles associated with the variation of each contribution in the directions of the columns and the rows (**C** and $\mathbf{S}^{\mathrm{T}}$, respectively). MCR-ALS solves Eq. (1), employing an alternating least squares (ALS) algorithm which iteratively calculates the concentration (**C**) and pure spectra ($\mathbf{S}^{\mathrm{T}}$) matrices, which optimally fit the experimental data matrix (**D**).

This optimization is carried out for a number of components established *a priori*, and using initial estimates of them, in either **C** or $\mathbf{S}^{\mathrm{T}}$. These estimates can be obtained using methods such as evolving factor analysis [43], SIMPLISMA [44] or the like. In order to ensure the physical sense of the results, several constraints can be applied to **C** and $\mathbf{S}^{\mathrm{T}}$ in the model during the ALS optimization; these include non-negativity and/or unimodality of the profiles, closure among chemical species, trilinearity of the entire matrix, selectivity and/or other shape or hard-modeling constraints [45,46].

Convergence of the model is achieved when the relative differences in the standard deviations of the residuals between experimental data and ALS calculated values in two consecutive iteration cycles, are less than a previously selected limit (usually 0.1%).

The evaluation of the figures of merit of the optimization helps to validate the overall procedure. The percentage of lack of fit, the percent of variance explained and the standard deviation of the residuals respect to experimental data are the main figures of merit for MRC-ALS.

The lack of fit is defined as the difference between the input information **D** and the results of the $\mathbf{CS}^{\mathrm{T}}$ product, obtained by MCR-ALS. These values are useful to understand whether experimental data were properly fitted by MCR-ALS and also to evaluate whether this fitting approached the PCA fit, a gold-standard decomposition method. A detailed calculation of the figures of merit was discussed elsewhere [39].

The quality of the resolution of Eq. (1) can be improved by carrying out simultaneous MCR-ALS analysis of multiple independent experiments run under different experimental conditions. Then, Eq. (1) can be extended to allow for the MCR-ALS simultaneous analysis of several experiments performed by the same spectroscopic technique. Eq. (2) shows the model for a two-experiment system, which resulted in the corresponding data matrices $\mathbf{D^1}$ and $\mathbf{D^2}$. Submatrices $\mathbf{C^1}$ and $\mathbf{C^2}$ contain the concentration profiles related to $\mathbf{D^1}$ and $\mathbf{D^2}$, respectively, $\mathbf{S}^{\mathrm{T}}$ is the common pure spectra matrix S and matrices $\mathbf{E^1}$ and $\mathbf{E^2}$ are the model errors related to each experiment.

$$\begin{bmatrix} \mathbf{D}^1 \\ \mathbf{D}^2 \end{bmatrix} = \begin{bmatrix} \mathbf{C}^1 \\ \mathbf{C}^2 \end{bmatrix} \mathbf{S}^{\mathrm{T}} + \begin{bmatrix} \mathbf{E}^1 \\ \mathbf{E}^2 \end{bmatrix} \quad (2)$$

This data arrangement is termed a column-wise augmented matrix; here, the resolved pure spectra are common to all experiments, whereas the concentration profiles can be different in each experiment. Advantageously, better species resolution can be achieved when both experiments are analyzed together instead of one by one, particularly in situations of rank deficiency [47,48].

On the other hand, when a chemical system is monitored using more than one spectroscopic technique, a row-wise augmented data-matrix can be built, where the individual data matrices,

corresponding to each spectroscopy, are organized one besides each other. Eq. (3) depicts the case of a chemical system monitored by two different spectroscopic techniques,

$$[\mathbf{D}_A,\ \mathbf{D}_B] = \mathbf{C}[\mathbf{S}_A^T,\ \mathbf{S}_B^T] + [\mathbf{E}_A,\ \mathbf{A}_B] \quad (3)$$

where $\mathbf{D}_A$ and $\mathbf{D}_B$ are the measurements obtained with the techniques A and B, respectively, for the same experiment. In this condition, $\mathbf{C}$ is a single matrix of concentration profiles, valid for both sets of raw measurements, whereas matrices $\mathbf{S}_A{}^T$ and $\mathbf{S}_B{}^T$ contain the calculated pure spectra of the participating species, for the techniques used in $\mathbf{D}_A$ and $\mathbf{D}_B$, respectively. Solving Eq. (3) for $\mathbf{C}$ and $[\mathbf{S}_A{}^T\mathbf{S}_B{}^T]$ provides an improved solution for all the species of the system, particularly if their spectra are not very different or lack signal in one of the two spectroscopies simultaneously analyzed.

The versatility of MCR-ALS is such that data analysis can be carried out with data acquired with different spectroscopies, resulting from the monitoring of multiple experiments. In this case, the augmentation of the data set has to be carried out both, column-wise and row-wise. The bilinear model for $\mathbf{n}$ experiments, studied by two different spectroscopies (A and B), is described by Eq. (4),

$$\begin{bmatrix} \mathbf{D}_A^1 & \mathbf{D}_B^1 \\ \vdots & \\ \mathbf{D}_A^n & \mathbf{D}_B^n \end{bmatrix} = \begin{bmatrix} \mathbf{C}^1 \\ \vdots \\ \mathbf{C}^n \end{bmatrix} [\mathbf{S}_A^T \mathbf{S}_B^T] + \begin{bmatrix} \mathbf{E}_A^1 & \mathbf{E}_B^1 \\ \vdots & \\ \mathbf{E}_A^n & \mathbf{E}_B^n \end{bmatrix} \quad (4)$$

where $\mathbf{D}_A^1$, the data matrix related to the first experiment, monitored by the technique A, accounts for the resolved concentration profiles submatrix $\mathbf{C}^1$, and a pure spectra submatrix, $\mathbf{S}_A^T$. This approach brings together the benefits of both previously described augmentations and delivers more reliable solutions, eventually removing rotational ambiguities and rank-deficiency problems. In addition, it improves the resolution of very complex data structures.

MCR-ALS is a second order chemometrics method, which has the ability to perform the determination of the analyte(s) in the presence of the unexpected/unknown interferent(s) in the prediction samples [49–51]; this property is known as the "second order advantage".

3. Results and discussion

3.1. Generation of the samples

In order to acquire a deeper insight into the processes involved during the thermal treatment of CIM, the drug was subjected to a series of experiments under carefully controlled conditions of time and temperature. The commercial polymorph A, which according to X-ray diffraction has the *syn*-imine configuration (Fig. 1) [18,34] was employed as source of the drug.

Exposure of CIM to various temperatures revealed that the drug melted without decomposition at 141–143 °C; increasing the temperature to 150 °C [29] for short periods of time exerted no significant effect on the stability or identity of the drug, as stemmed from NMR analysis. However, when CIM was thermally stressed by heating to 160–180 °C (for 80 and 35 min, respectively), it afforded a liquid, which solidified upon cooling to yield a tannish glassy material. Prolonged exposure of the drug to temperatures above 180 °C caused its decomposition.

Interestingly, previous NMR studies found no evidence for prototropic tautomerization or general exchange of the NH hydrogens among disubstituted *N*-aryl-*N*′-cyanoguanidines, even at elevated temperatures. This was attributed to the strongly electron-withdrawing cyano group, which reduces the acid–base character of the cyanoguanidine moiety and the rate of prototropic tautomerization [35,52].

The samples resulting from thermal treatments at 160 °C and 180 °C were examined microscopically and spectroscopically (Ultraviolet, FTIR and NMR).

3.2. Optical microscopy of the pre-melted solid

Observation of pre-melted glassy solid samples of CIM, under normal and polarized light, revealed the lack of a crystalline structure, even after leaving the solid samples at room temperature for several days.

3.3. Ultraviolet and FTIR spectra of the pre-melted solid

The UV spectra of the pre-melted solids, dissolved in MeOH, exhibited only minor shape differences with regards to that of pure CIM. Analogously, their FTIR spectra were almost indistinguishable from that of CIM, except for the 771.5–829.4 cm^{-1} region, in the fingerprint zone. Absorptions in this zone are attributed to N—H

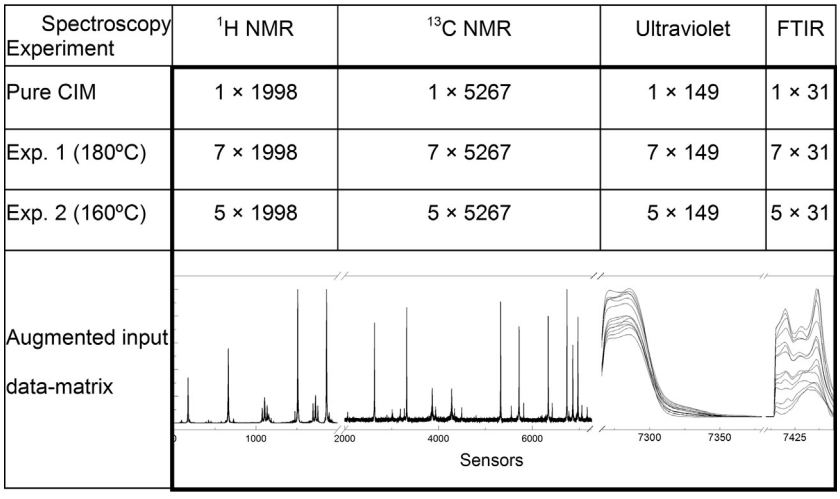

Fig. 2. Schematics of the architecture of the augmented input data-matrix. Dimensions of the vectors are row × column.

bending (wagging) [53]; thus, the observed changes suggested tautomerization of the drug.

3.4. Multi-spectroscopic/chemometric approach to the analysis of the kinetics of the transformation

Due to its versatility, MCR-ALS is gaining wide acceptance as a chemometrics tool, suitable for extracting information from complex dynamic systems. MCR-ALS has been applied to the analysis of various evolving mixtures, in order to gain knowledge about their components and corresponding abundances in the samples [54–56]. The theoretical background of its operation has been described in Section 2.9.

It was expected that the second order advantage property of MCR-ALS could allow to determine the level of CIM in the presence of *a priori* unknown interferents (TAU and other secondary products) and to deconvolve the spectral and concentration profiles of the interferent. However, MCR-ALS-mediated analyses of neither the UV or FTIR spectra of the mixtures afforded satisfactory results, both being unable to provide meaningful information on the time-evolution and identity of the species in the heat-treated samples. This was attributed to rotational ambiguity, since the observed differences were only minor in nature. This precluded the usage of these spectroscopies as single suitable tools for monitoring the effects of heat on CIM. Furthermore, their combined use was also unable to shed light on the thermal degradation process.

Therefore, NMR (^{1}H and ^{13}C) data were added and the study of the kinetics of the thermal process was approached by MCR-ALS analysis of an augmented data-matrix.

The ^{1}H NMR data sets used were previously normalized, conveniently aligned, polished to exclude the non-informative regions and finally their resolution was reduced by diminishing the number of sensors to 50% in order to ease calculations.

The pre-processed signal matrices were augmented stepwise. First, matrix coupling was performed with data of the same experiment in the direction of the rows (row-wise) to give two matrices with their data arranged in following order: ^{1}H NMR, ^{13}C NMR, ultraviolet and infrared. Secondly, the matrices corresponding to each experiment were joined column-wise, placing the data of the initial time (pure CIM) atop of them, as shown in Fig. 2.

Inspection of a scree plot [57] resulting from principal component analysis (PCA) of the augmented input matrix revealed that two components sufficed to explain 98.6% of the variance of the system. Therefore, the MCR-ALS algorithm was initialized with only two vectors, the polished combined spectrum of pure CIM (Fig. 2) and a noise vector, prepared by subtracting the combined spectra of CIM from the combined spectra of the most degraded sample. Interestingly, no additional meaningful components were found when the MCR algorithm was initialized with three components, demonstrating the stability and consistency of the deconvolution method.

In order to convey physical meaning to the results, three restrictions were put in place before starting the computations. One of them was 'non-negativity' in the spectral and concentration domains, based on the facts that the expected concentrations of CIM, the degradation products, and their NMR spectra should all be positive. Another restriction imposed was 'unimodality' of the concentration values, requiring the concentration profiles of the analytes to contain only one maximum. The third stipulation was the 'closure' condition, put in place to guarantee that the sum of the abundances analytes remains constant. The latter requirement was based on literature precedents [32,34], indicating that CIM samples do not lose weight in the studied temperature range, and meaning that the total number of moles of the intervening species (CIM and concomitantly formed impurities) remains constant during the thermal process.

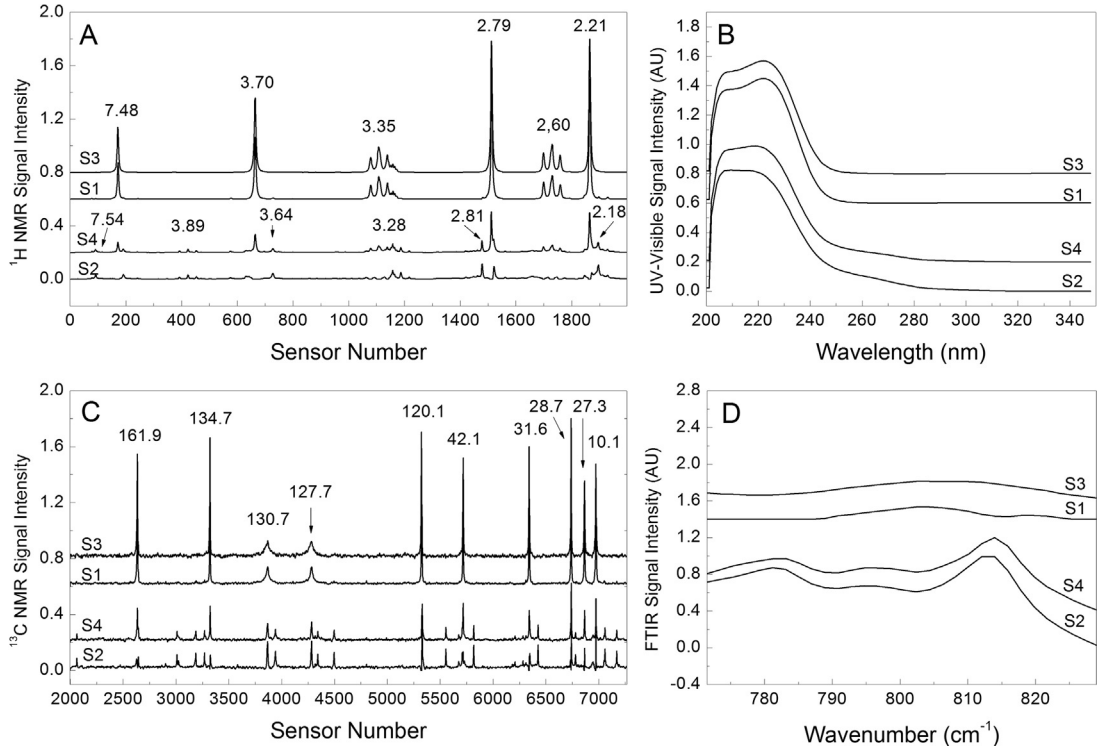

Fig. 3. Comparison between the MCR-ALS spectral output vectors (S1 and S2) with the input vector corresponding to authentic CIM (S2) and a heavily degraded sample (S4), along their four spectral components: (A) ^{1}H NMR; (B) UV (C) ^{13}C NMR and (D) FTIR. NMR chemical shift data are in ppm.

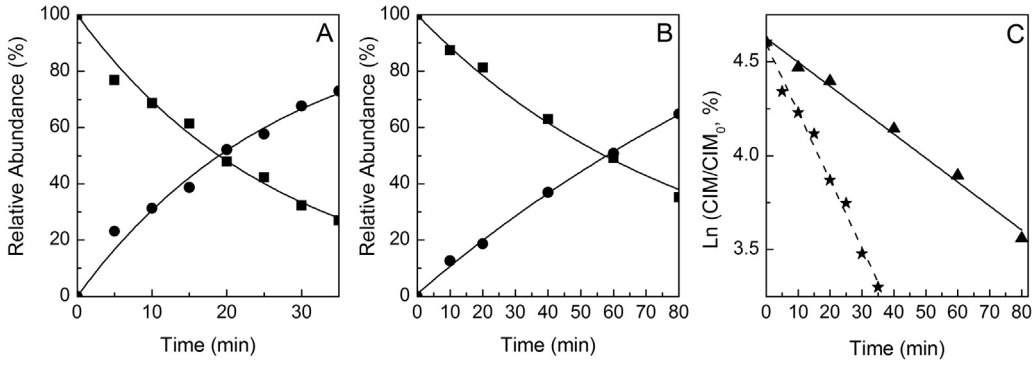

Fig. 4. Evolution of the abundances of CIM (■) and its degradation products (NEWP, ●) over time, according to the MCR-ALS algorithm. (A) at 180 (B) at 160 °C semilogarithmic plot of the evolution of the abundances of CIM at 180 °C (★) and 160 °C (▲).

Once the initial conditions were established, the MCR-ALS algorithm was used to deconvolute the input matrix. MCR-ALS solved the individual contributions of the two main components to the whole process over time and afforded both, spectral information of the species involved (S1 and S2) and the corresponding time-dependent evolution of their abundances (C1 and C2).

Fig. 3 displays the ^{1}H NMR, ^{13}C NMR, UV and FTIR spectra of authentic CIM (S3) along with the MCR-ALS spectral output vectors (S1 and S2) for the main components of the samples, and the data of a heavily degraded sample (S4), acquired with the same spectroscopic tools.

The comparison of the output spectral vectors (S1 and S2) with the spectrum of authentic CIM (S3) by linear regression revealed a greater correspondence between the latter with S1 (adjusted $r^2 = 0.95$, $n = 7445$) than with S2 (adjusted $r^2 = 0.22$). This allowed the unequivocal confirmation of the API as one of the components of the mixtures (Fig. 3). The corresponding concentration vector (C1) granted information useful to attribute the contribution of CIM in the different samples at both test temperatures (Fig. 4A).

The spectra of the other component (S2, Fig. 3) suggested the time-dependent formation (C2) of a main degradation product along with other (unidentifiable) impurities (analyzed together as NEWP). Interestingly, however, the fact that only two components were detected may be better attributed to the concomitant formation of one main degradant and the other impurities rather than being a result of the scarce number of time-points employed.

In order to ensure the validity of the results, the figures of merit of the model were evaluated. In a first step the lack of fit of the MCR-ALS algorithm (16.8%) was compared to the lack of fit of PCA (11.6%) in the decomposition of the dataset. Both figures were of the same order and in agreement with the experimental noise which should be expected to arise from a dataset composed by four analytical technics and two different experimental conditions.

The similarity of both lack of fit values (PCA and MCR-ALS) also evidenced that the selected constraints (non-negativity on the spectral and concentration profiles and unimodality and closure of the concentration profiles) were applied on sound physicochemical grounds and were not merely arbitrary restrictions.

In addition, the MCR-ALS method proved to be robust, since small changes in the initial conditions did not render any significant changes in the number of components, the number of iterations (5–10) and the variance explained by the model ($r^2 > 97\%$).

Fig. 4A and B revealed that approximately 70% of CIM was degraded during both experiments. According to the multi-spectroscopic/MCR-ALS approach, the disappearance of CIM and simultaneous emergence of the new products (NEWP) seemed to follow a first order kinetics (Eqs. (5) and (6), where [CIM$_0$] is the abundance of CIM at the beginning of the experiment).

The rate order was confirmed by fitting zero, first and second order models (Table 1) to the data of the samples, heated both at 180 and 160 °C, and examining the adjusted r^2 of the fitted models, the corresponding distribution of the residuals and the values of the Akaike information criterion (AIC) [58].

It was observed that the first order curve exhibited the highest value of r^2, the lowest value of AIC, and the residues displayed a random distribution. Furthermore, the semilogarithmic plots of the decrease of CIM (Fig. 4C) adjusted straight lines ($r = 0.996$ and 0.995 at 160 °C and 180 °C, respectively). Therefore, it was concluded that the process has a first order kinetics.

$$[\text{CIM}, \%] = [\text{CIM}_0] \times e^{-kt} \quad (5)$$

$$[\text{NEWP}, \%] = [\text{CIM}_0] \times (1 - e^{-kt}) \quad (6)$$

$$\ln\left(\frac{k_{T_1}}{k_{T_2}}\right) = \left(\frac{E_a}{R}\right) \times \left(\frac{1}{T_2} - \frac{1}{T_1}\right) \quad (7)$$

Table 1
Kinetic equations of the degradation of CIM. Statistical parameters.

Temp. (°C)	Order/equations	Zero $[C] = [C]_0 - k \times t$	First $[C] = [C]_0 - e^{-k \times t}$	Second $[C] = [C]_0/[1 - [C]_0 \times k \times t]$
	Parameters			
160 °C	k	0.0085 ± 0.0003	0.0121 ± 0.0004	0.0167 ± 0.0016
	Adjusted r^2	0.9873	0.9935	0.9633
	AIC	−36.1	−40.2	−29.8
180 °C	k	0.023 ± 0.001	0.037 ± 0.001	0.055 ± 0.004
	Adjusted r^2	0.924	0.985	0.966
	AIC	−37.8	−50.9	−44.3

$$t_{1/2} = \frac{0.693}{k} \quad (8)$$

Application of the Arrhenius equation (Eq. (7)), where k_{T1} and k_{T2} are the rate constants at temperatures T_1 and T_2, respectively and R is the gas constant, and the formula of Eq. (8) enabled the estimation of the activation energy (E_a) of the process and the half-life times ($t_{1/2}$) of the conversion of CIM at different temperatures, respectively. The results are summarized in Table 2.

3.5. NMR data analysis of the pre-melted solid. Structural elucidation of TAU

The structure of the main thermally-generated impurity was confirmed to be the N_3-enamino tautomer of the drug (TAU), after an exhaustive NMR spectral analysis of its mixtures with CIM. TAU was produced concomitantly with other unidentified degradation products and could not be separated from them.

Taking into account the most relevant signals of the ^{1}H NMR spectrum (Fig. 5), it was observed that the resonances of the newly generated product closely resembled those of CIM, suggesting that both are closely related compounds (Fig. 1).

The ^{1}H NMR spectrum of the product revealed a couple of singlets at 2.18 and 2.81 ppm (3H each), which were assigned to H-4 and H-9, the methyl groups substituting the imidazole moiety and N_4, respectively. Two additional singlets at δ 3.64 (2H) and δ 7.54 (1H) were attributed to H-5 and H-1, respectively.

In addition, a pair of coupled (J = 7.1 Hz) double doublets resonating at δ 3.28 and 3.89 (2H each) were observed, which were assigned to H-6 and H-7, respectively. Since H-6 is partially overlapped with H-7 of CIM and the residual methyl protons of MeOH-d_4, the characteristics of this spin system were fully confirmed by COSY and TOCSY experiments. The TOCSY experiment creates correlations between all protons within a given spin system. However, TOCSY experiments run on signals of the impurities did not provide any useful connectivity information, being helpless in the effort to characterize other concomitantly formed products.

The ^{13}C NMR spectrum of the mixture enriched in TAU (Fig. 6) exhibited ten relevant new signals, three of which (δ 8.7, 31.0 and 135.1) were confirmed to belong to methyl/methine carbons by a DEPT 135 experiment, and assigned to C-4, C-9 and C-1, respectively.

Three additional high-field signals resonating at 28.4, 35.5 and 60.4 ppm were attributed to C-5, C-6 and C-7, respectively, two resonances (126.0 and 135.5) were assigned to the remaining carbons of the imidazole ring, while the remaining pair of signals were attributed to the cyanoguanidine moiety [1261 (C-10) and 1661 (C-8)].

All the C—H correlations, particularly the diagnostic H-7/C-7 pair of signals (3.89/60.4 ppm), were confirmed by an HSQC spectrum. On the other hand, long-range H—C correlations deduced from the analysis of the HMBC spectrum, confirmed the integrity of the original drug skeleton. Table 3 displays the assignments of the ^{1}H and ^{13}C resonances of CIM and TAU, as well as the correlations observed in the HMBC spectrum.

Table 2
Summary of the characteristics of the thermal degradation process of CIM.

T (°C)	T (°K)	k (min^{-1})	n	$t_{1/2}$ (min)	E_a (Kcal mol^{-1})
180	453	0.04	8	19.0	22.3
160	433	0.012	6	59.4	

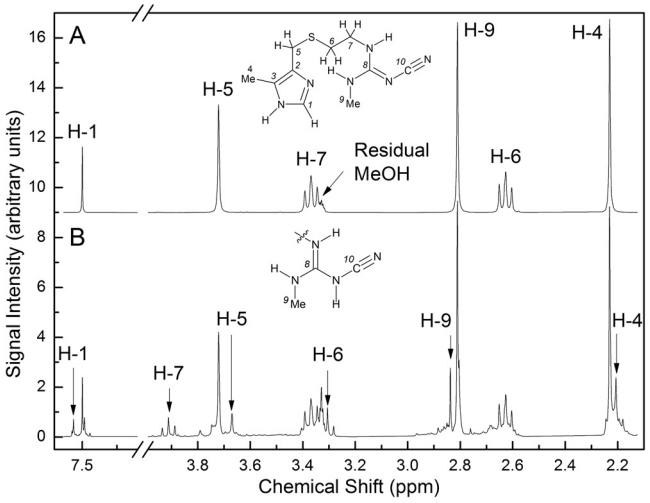

Fig. 5. ^{1}H NMR spectra of (A) pure CIM and (B) the mixture of CIM and other products, containing TAU.

Final scrutiny of the places where the major chemical shift differences took place in the ^{1}H (H-6 and H-7) and ^{13}C (C-6, C-7, C-8 and C-10) spectra confirmed the formation of the proposed tautomer.

The signal assignments of Table 3 agree with the proposal of TAU as an N_3-enamine tautomer of CIM (Fig. 1). However, owing to the possibility of *syn*/*anti* geometrical isomerism on N_3 [59], the structure of TAU may correspond to either isomer **X2** (*anti*) or **X5** (*syn*). Efforts were placed to identify which one of these isomers is TAU. Therefore, nuclear Overhauser effect (NOE) experiments were run, with the aim of observing interactions between H-9 and H-7.

No signal intensifications were evidenced (Fig. 7); however, this outcome turned out to be non-conclusive, because a control experiment with CIM revealed the lack of NOE enhancements when the analogous positions (H-9 and H-7) were irradiated. Most probably, these results reflect that in the preferred conformation of CIM its methyl group remains spatially distant from H-7 in order to minimize steric interactions. Analogously, for TAU the results are compatible with structures **I′** and **II**, corresponding to both of its possible geometrical isomers.

Interestingly, many studies have been carried out with CIM at temperatures above its melting point; however, its tautomer has

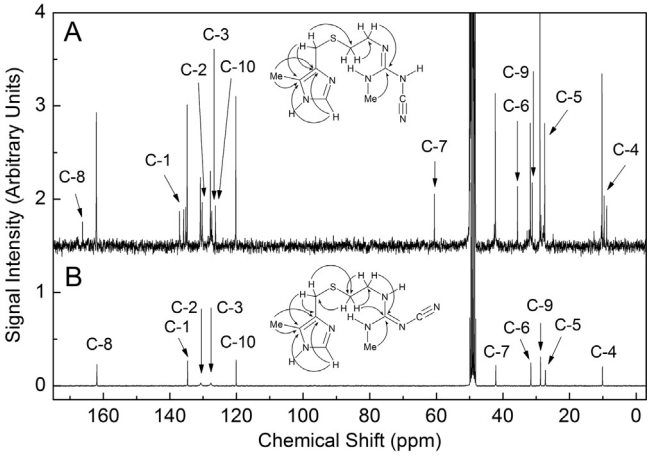

Fig. 6. ^{13}C NMR spectra of (A) a heavily degraded sample of CIM containing TAU and other products and (B) pure CIM. The inserted chemical structures depict the long-range H–C correlations obtained by the HMBC experiment.

Table 3
NMR signal assignments (H and C) of CIM and TAU, employing 1D (^{1}H and ^{13}C) and 2D (HSQC and HMBC) experiments.

H/C N°	Cimetidine				Tautomer of CIM			
	^{1}H	^{13}C	HSQC[a]	HMBC[b]	^{1}H	^{13}C	HSQC[a]	HMBC[b]
1	7.48 (s)	134.7	+	C_2; C_3	7.44 (s)	135.1	+	C_2; C_3
2		130.7				135.1		
3		127.7				126.0		
4	2.21 (s)	10.1	+	C_2; C_3	2.18 (s)	8.7	+	C_2; C_3
5	3.70 (s)	27.3	+	C_2; C_3; C_6; C_{10}	3.64 (s)	28.4	+	C_2; C_3; C_6
6	2.60 (dd, J = 7.1)	31.6	+	C_5; C_7	3.28 (dd, J = 7.1)	35.5	+	C_7
7	3.35 (dd, J = 7.1)	42.1	+	C_6; C_8	3.89 (dd, J = 7.1)	60.4	+	C_8
8		161.9				166.1		
9	2.79 (s)	28.7	+	C_8	2.81 (s)	31.0	+	C_8
10		120.1				126.1		
NH								

[a] The + sign indicates that a cross-peak was observed.
[b] Carbon atoms exhibiting cross-peaks with the observed H-atom.

never been reported. This should not be surprising, since the previous investigations involved thermal and microscopic approaches, such as thermogravimetry, DSC and polarized light optical microscopy [31–34], which are insensitive to this kind of transformation. The former because no mass change takes place during the process, while the sensitivity of the latter two is probably unsuitable to detect the tautomeric conversion.

3.6. Theoretical studies and proposed mechanism for the transformation

The marked stability of TAU in solution (weeks in MeOH) was puzzling. Therefore, and in order to find the basis of such stability an in depth bibliographic revision and a set of theoretical calculations were carried out.

The theoretical study was carried out on CIM and TAU at the B3LYP 6-31 + G(D) level in order to enquire into their relative stabilities. Analysis of the results revealed that TAU is 21 kcal mol^{-1} less stable than CIM, arbitrary placed at a 0 kcal mol^{-1} level (Fig. 8A). It was also found that the energy barrier for the conversion between CIM and its tautomer is 46 kcal mol^{-1} in the direct sense and 25 kcal mol^{-1} in the reverse direction; these barriers are too high for tautomer interconversion at room temperature.

The above structural information is referred exclusively to isolated molecules in the gas phase. Since it cannot be transferred directly to the solid state or to the melted drug, comparing these data with experimental values obtained for the solid forms should be done with due care.

These results, which are fully consistent with those found for the unsubstituted cyanoguanidine isomers (Fig. 8B), helped to detect the key features of the isomerism of the cyanoguanidine moiety. It was found that the 'cyanoimine' and 'cyanoamine' forms of cyanoguanidine are stable tautomers [60], with the former tautomer being 11.6 kcal mol^{-1} more stable. The potential barrier of 45.3 kcal mol^{-1} found between the tautomers also resulted too high for their room temperature interconversion.

From the mechanistic point of view, the discussed tautomerization formally involves a [1,3]-hydrogen shift, which may take place through intramolecular proton transfer, mutual transfer within a dimer or concerted transfer *via* a cyclic structure [61]. It may also possibly involve a previous *syn–anti* isomerization of the cyanoimine double bond, a process which entails a transition state energy of 23.1 kcal mol^{-1} in case of cyanoguanidine [51].

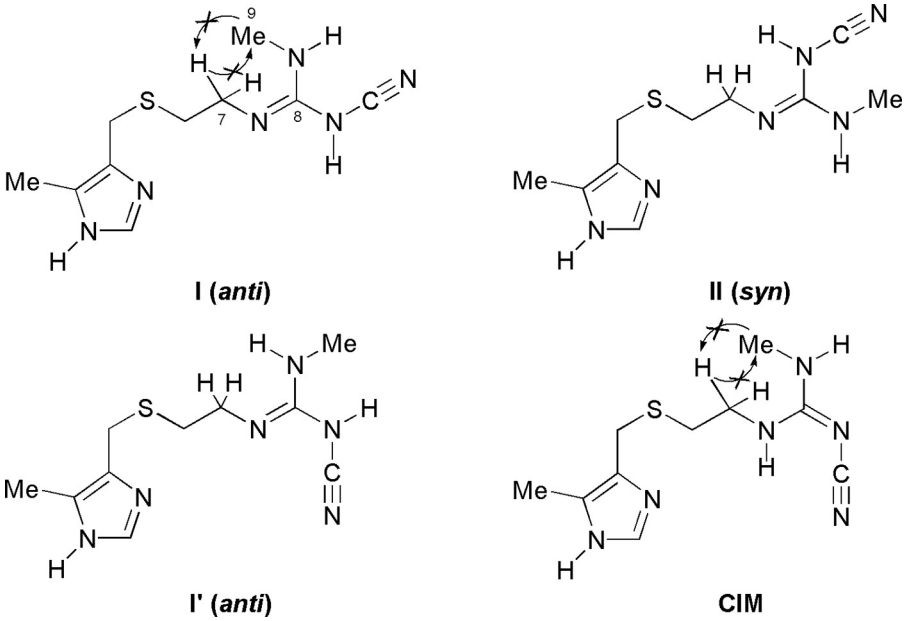

Fig. 7. Chemical structures of CIM, the geometrical isomers of TAU (**I** and **II**) and the expected NOE signal enhancements between H-9 and H-7. Structure **I′** is a conformer of **I**.

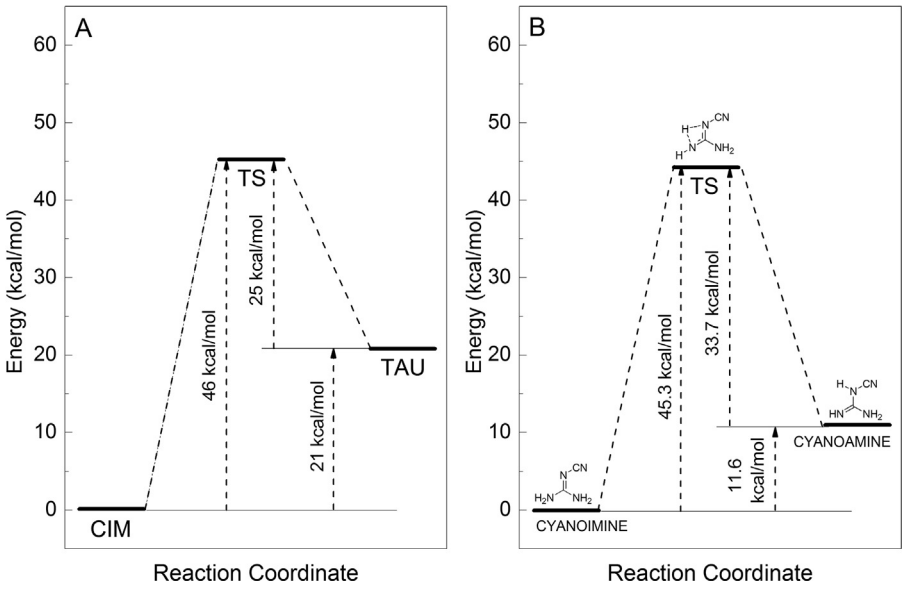

Fig. 8. Diagram of energy levels of CIM and TAU (A). Comparison with cyanoguanidine (B) [51].

On the other side, the related N_4-enamino tautomer could also be concomitantly formed. However, it could be less stable, either reverting to CIM or decomposing into unidentified degradation products, such as those formed along with TAU. Although many analogous tautomerization processes take place with easy reversion, examples have been found where the tautomers may coexist for years until complete conversion to the most stable species is completed [8].

4. Conclusions

In conclusion, it has been demonstrated that heating anhydrous cimetidine (CIM) at temperatures between 160 °C and 180 °C causes its partial transformation, leading to the stable and hitherto undisclosed N_3-enamino tautomer (TAU) and other still unidentified species. UV and FTIR spectral data of TAU exhibited only minor differences with regards to those of CIM, while mono- and two-dimensional ^{1}H and ^{13}C NMR spectral data allowed the unambiguous elucidation of the structure of the compound.

The level of CIM was determined in the presence of *a priori* unknown inteferents (TAU and other secondary products) using the second order advantage of MCR-ALS. In addition, this advantage was exploited to deconvolve the spectral and concentration profiles of the interferent (TAU), to confirm its spectral characteristics and to evaluate the kinetics of its formation. The rate of the thermal degradation of CIM was determined, and demonstrated to follow a first order kinetics. Half-life times and the Arrhenius activation energy of the process were also determined.

In addition, a quantum mechanical study was carried out on the tautomers of CIM, employing the density function theory (DFT) at the HF/6-311 + G**, B3LYP/3-21 + G* and B3LYP/6-311 + G** levels. This revealed that the 'imino' form of the drug is more stable than the N_3-enamino tautomer. Furthermore, the potential barriers for the direct and reverse conversion between both tautomers, due to breaking and forming N—H bonds with concomitant displacement of a double bond, are too high (46 and 25 kcal mol^{-1}, respectively) for their room temperature interconversion.

Two main consequences and a lesson could result from the above findings. Among the consequences, it should be mentioned that correlation of thermal data from samples of CIM at temperatures above its melting point must be done with due care [62]. On the other hand, improvement of the preparation method and a proper separation of TAU may result in a new chemical entity, with high potential of being bioactive or otherwise useful. On the side of the lesson, it should be learned that no matter how much effort is placed in studying APIs, their chemistry is usually so rich that new related and potentially relevant products may be found if new analytical techniques or novel approaches are used.

Acknowledgements

The authors are thankful to Consejo Nacional de Investigaciones Científicas y Tecnológicas (CONICET), Agencia Nacional de Promoción Científica y Tecnológica (ANPCyT), Secretaría de Ciencia Tecnología e Innovación (SECTeI) and Secretaría de Ciencia y Tecnología de la UNR (SECyT-UNR) for financial support. NLC and SOS acknowledge CONICET for their fellowships.

References

[1] D. Jain, P.K. Basniwal, Forced degradation and impurity profiling: recent trends in analytical perspectives, J. Pharm. Biomed. Anal. 86 (2013) 11–35.
[2] ICH Harmonized Guideline: Impurities in New Drug Substances Q3A (R2), ICH Steering Committee, Geneva, Switzerland, 2006.
[3] ICH Harmonized Guideline: Impurities in New Drug Products Q3B (R2), ICH Steering Committee, Geneva, Switzerland, 2006.
[4] The United States Pharmacopeia, USP36-NF31, Impurities in Drug Substances and Drug Products, U.S. Pharmacopeial Convention Inc., Rockville, MD, USA, 2013 (Chapter 1086).
[5] K.R. Wadekar, M. Bhalme, S. Srinivasa Rao, K. Vigneshwar Reddy, L. Sampath Kumar, E. Balasubrahmanyam, Evaluating impurities in drugs (Part I of III), Pharm. Technol. 36 (2012) 46–51.
[6] P. Ferraboschi, D. Colombo, M. De Mieri, P. Grisenti, Evaluation, synthesis and characterization of tacrolimus impurities, J. Antibiot. 65 (2012) 349–354.
[7] A.R. Katritzky, C.D. Hall, B.-D. El-Gendy, B.B. Draghici, Tautomerism in drug discover, J. Comput. Aided Mol. Des. 24 (2010) 475–484.
[8] Z. Wojnarowska, P. Wlodarczyk, K. Kaminski, K. Grzybowska, L. Hawelek, M. Paluch, On the kinetics of tautomerism in drugs: new application of broadband dielectric spectroscopy, J. Chem. Phys. 133 (094507) (2010) 1–9.
[9] W.A. Hoogerwerf, J. Pasricha, Pharmacotherapy of gastric acidity, peptic ulcers, and gastroesophageal reflux disease, in: L.L. Brunton, J.S. Lazo, K.L. Parker (Eds.), Goodman & Gilman's The Pharmacological Basis of Therapeutics, 11th ed., McGraw-Hill, New York, 2006, pp. 967–981.
[10] Martindale: The Complete Drug Reference, in: S.C. Sweetman (Ed.), 34nd ed., Pharmaceutical Press, London, UK, 2005.

[11] K. Arae, K. Oboki, T. Ohno, M. Hirata, S. Nakae, H. Taguchi, H. Saito, T. Nakajima, Cimetidine enhances antigen-specific IgE and Th2 cytokine production, Allergol. Int. 60 (2011) 339–344.

[12] F. Lefranc, P. Yeaton, J.R. Brotchi. Kiss, Cimetidine, an unexpected anti-tumor agent, and its potential for the treatment of glioblastoma, Int. J. Oncol. 28 (2006) 1021–1030.

[13] M. Kubecova, K. Kolostova, D. Pinterova, G. Kacprzak, V. Bobek, Cimetidine: an anticancer drug? Eur. J. Pharm. Sci. 42 (2011) 439–444.

[14] H. Ishikura, H. Fukui, N. Takeyama, T. Tanaka, Cimetidine activates interleukin-12, which enhances cellular immunity, Blood 93 (1999) 1782–1783.

[15] N. Scheinfeld, Cimetidine: a review of the recent developments and reports in cutaneous medicine, Dermatol. Online J. 9 (2003) 4–9.

[16] E. Hädicke, F. Frickel, A. Franke, Die Struktur von Cimetidin (*N*″-cyan-*N*-methyl-*N*′-[2-[(5-methyl-1*H*-imidazol-4-yl)methylhio]ethyl]guanidin), einem Histamin H2-Rezeptor-Antagonist, Chem. Ber. 111 (1978) 3222–3232.

[17] L. Parkanyi, A. Kalman, B. Hegedus, K. Harsanyi, J. Kreidl, Structure of a novel and reproducible polymorph (Z) of the histamine H2-receptor antagonist cimetidine, C10H16N6S, Acta Crystallogr. C40 (1984) 676–679.

[18] R.J. Cernik, A.K. Cheetham, C.K. Prout, D.J. Watkin, A.P. Wilkinson, B.T.M. Willis, The structure of cimetidine ($C_{10}H_{16}N_6S$) solved from synchrotron-radiation X-ray powder diffraction data, J. Appl. Crystallogr. 24 (1991) 222–226.

[19] G. Karpinska, J.C. Dobrowolski, A.P. Mazurek, Conformation and tautomerism of the cimetidine molecule: a theoretical study, J. Mol. Struct. 645 (2003) 37–43.

[20] G.J. Durant, J.C. Emmett, C.R. Ganellin, P.D. Miles, M.E. Parsons, H.D. Prain, G.R. White, Cyanoguanidine–thiourea equivalence in the development of the histamine H2-receptor antagonist, Cimetidine, J. Med. Chem. 20 (1977) 901–906.

[21] A. Arakcheeva, P. Pattison, A. Bauer-Brandl, H. Birkedal, G. Chapuis, Cimetidine, $C_{10}H_{16}N_6S$, form C: crystal structure and modelling of polytypes using the superspace approach, J. Appl. Crystallogr. 46 (2013) 99–107.

[22] D.A. Middleton, C.S. Le Duff, X. Peng, D.G. Reid, D. Saunders, Molecular conformations of the polymorphic forms of cimetidine from ^{13}C solid-state NMR distance and angle measurements, J. Am. Chem. Soc. 122 (2000) 1161–1170.

[23] D.R. Ellis, M.E. Palmer, L.W. Tetler, C. Eckers, Separation of cimetidine and related materials by aqueous and non-aqueous capillary electrophoresis, J. Chromatogr. A 808 (1998) 269–275.

[24] P. Betto, E. Ciranni-Signoretti, R. Di Fava, Determination of cimetidine and related impurities in pharmaceutical formulations by high-performance liquid chromatography, J. Chromatogr. 586 (1991) 149–152.

[25] N. Helali, L. Monser, Simultaneous determination of cimetidine and related compounds in pharmaceuticals by HPLC on a porous graphitic carbon column, Chromatographia 63 (2006) 425–430.

[26] Z. Halmos, C. Szantay Jr., J. Brlik, A. Csehi, K. Varga, P. Horvdth, M. Kislaki, Gy. Domány, A. Nemes, S. Görög, Estimation of impurity profiles of drugs and related materials. Part 15. Identification of minor impurities in cimetidine, J. Pharm. Biomed. Anal. 15 (1996) 1–5.

[27] E.H. Evans, J.-C. Wolff, C. Eckers, Sulfur-specific detection of impurities in cimetidine drug substance using liquid chromatography coupled to high resolution inductively coupled plasma mass spectrometry and electrospray mass spectrometry, Anal. Chem. 73 (2001) 4722–4728.

[28] A. Bauer-Brandl, Polymorphic transitions of cimetidine during manufacture of solid dosage forms, Int. J. Pharm. 140 (1996) 195–206.

[29] M. Otsuka, F. Kato, Y. Matsuda, Physicochemical stability of cimetidine amorphous forms estimated by isothermal microcalorimetry, AAPS PharmSciTech 3 (4) (2002) 32–44 article 30.

[30] N.L. Calvo, R.M. Maggio, T.S. Kaufman, A dynamic thermal ATR-FTIR/chemometrics approach to the analysis of polymorphic interconversions. Cimetidine as a model drug, J. Pharm. Biomed. Anal. 92 (2014) 90–97.

[31] G.L. Perpétuo, D.A. Gálico, R.A. Fugita, R.A.E. Castro, M.E.S. Eusébio, O. Treu-Filho, A.C.M. Silva, G. Bannach, Thermal behavior of some antihistamines, J. Therm. Anal. Calorim. 111 (2013) 2019–2028.

[32] F.S. Souza, R.O. Macedo, J.W.E. Veras, Studies of cimetidine preformulated and tablets for TG and DSC coupled to the photovisual system, Thermochim. Acta 392–393 (2002) 99–106.

[33] S. Yamamura, H. Gotoh, Y. Sakamoto, Y. Momose, Physicochemical properties of amorphous salt of cimetidine and diflunisal system, Int. J. Pharm. 241 (2002) 213–221.

[34] M. Shibata, H. Kokubo, K. Morimoto, K. Morisaka, T. Ishida, M. Inoue, X-ray structural studies and physicochemical properties of cimetidine polymorphism, J. Pharm. Sci. 72 (1983) 1436–1442.

[35] I. Ghiviriga, B.D. El-Gendy, P.J. Steel, A.R. Katritzky, Tautomerism of guanidines studied by (15)N NMR: 2-hydrazono-3-phenylquinazolin-4(3*H*)-ones and related compounds, Org. Biomol. Chem. 7 (2009) 4110–4119.

[36] R.M. Maggio, N.L. Calvo, S.E. Vignaduzzo, T.S. Kaufman, Pharmaceutical impurities and degradation products: uses and applications of NMR techniques, J. Pharm. Biomed. Anal. 101 (2014) 102–122.

[37] C. Fernández, M.P. Callao, M.S. Larrechi, UV–visible-DAD and ^1H NMR spectroscopy data fusion for studying the photodegradation process of azo-dyes using MCR-ALS, Talanta 117 (2013) 75–80.

[38] E. Bezemer, S. Rutan, Resolution of overlapped NMR spectra by two-way multivariate curve resolution alternating least squares with imbedded kinetic fitting, Anal. Chim. Acta 459 (2002) 277–289.

[39] J. Jaumot, R. Gargallo, A. de Juan, R. Tauler, A graphical user-friendly interface for MCR-ALS: a new tool for multivariate curve resolution in MATLAB, Chemometr. Intell. Lab. Syst. 76 (2005) 101–110.

[40] G. Tomasi, F. van den Berg, C. Andersson, Correlation optimized warping and dynamic time warping as preprocessing methods for chromatographic data, J. Chemometr. 18 (2004) 231–241.

[41] M.J. Frisch, G.W. Trucks, H.B. Schlegel, G.E. Scuseria, M.A. Robb, J.R. Cheeseman, G. Scalmani, V. Barone, B. Mennucci, G.A. Petersson, H. Nakatsuji, M. Caricato, X. Li, H.P. Hratchian, A.F. Izmaylov, J. Bloino, G. Zheng, J.L. Sonnenberg, M. Hada, M. Ehara, K. Toyota, R. Fukuda, J. Hasegawa, M. Ishida, T. Nakajima, Y. Honda, O. Kitao, H. Nakai, T. Vreven, Montgomery Jr. J.A, F. J.E. Peralta, M. Ogliaro, J.J. Bearpark, E. Heyd, K.N. Brothers, V.N. Kudin, R. Staroverov, J. Kobayashi, K. Normand, A. Raghavachari, J.C. Rendell, S.S. Burant, J. Iyengar, M. Tomasi, N. Cossi, J.M. Rega, M. Millam, J.E. Klene, J.B. Knox, V. Cross, C. Bakken, J. Adamo, R. Jaramillo, R.E. Gomperts, O. Stratmann, A.J. Yazyev, R. Austin, C. Cammi, J.W. Pomelli, R.L. Ochterski, K. Martin, V.G. Morokuma, G.A. Zakrzewski, P. Voth, J.J. Salvador, S. Dannenberg, A.D. Dapprich, O. Daniels, J.B. Farkas, J.V. Foresman, J. Ortiz, D.J. Cioslowski, Fox Gaussian 09, Rev. A.1, Gaussian, Inc., Wallingford CT, 2009.

[42] R. Tauler, Multivariate curve resolution applied to second-order data, Chemometr. Intell. Lab. Syst. 30 (1995) 133–146.

[43] M. Maeder, Evolving factor analysis for the resolution of overlapping chromatographic peaks, Anal. Chem. 59 (1987) 527–530.

[44] W. Windig, J. Guilment, Interactive self-modeling mixture analysis, Anal. Chem. 63 (1991) 1425–1432.

[45] R. Tauler, A.K. Smilde, B.J. Kowalski, Selectivity local rank, 3-way data analysis and ambiguity in multivariate curve resolution, J. Chemometr. 9 (1995) 31–58.

[46] A. de Juan, R. Tauler, Chemometrics applied to unravel multicomponent processes and mixtures: revisiting latest trends in multivariate resolution, Anal. Chim. Acta 500 (2003) 195–210.

[47] M. Amrhein, B. Srinivasan, D. Bonvin, M.M. Schumacher, On the rank deficiency and rank augmentation of the spectral measurement matrix, Chemometr. Intell. Lab. Syst. 33 (1996) 17–33.

[48] J. Saurina, S. Hernández-Cassou, R. Tauler, A. Izquierdo-Ridorsa, Multivariate resolution of rank-deficient spectrophotometric data from first-order kinetic decomposition reactions, J. Chemometr. 12 (1998) 183–203.

[49] R. Bro, Multi-way Analysis in the Food Industry (Ph.D. thesis), Universiteit van Amsterdam, 1998.

[50] K.S. Booksh, B.R. Kowalski, Theory of analytical chemistry, Anal. Chem. 66 (1994) 782A–791A.

[51] B.J. Prazen, R.E. Synovec, B.R. Kowalski, Standardization of second order chromatographic/spectroscopic data for optimum chemical analysis, Anal. Chem. 70 (1998) 218–225.

[52] I.D. Cunningham, N.C. Wan, B.G. Cox, ^1H and ^{15}N NMR studies of *N*-substituted-*N*′-cyanoguanidines, J. Chem. Soc. Perkin Trans. 2 (1994) 1849–1853.

[53] A.E. Aliaga, C. Garrido, P. Leyton, G. Díaz, J.S. Gómez-Jeria, T. Aguayo, E. Clavijo, M.M. Campos-Vallette, S. Sánchez-Cortés, SERS and theoretical studies of arginine, Spectrochim. Acta A 76S (2010) 458–463.

[54] R.M. Maggio, M.A. Rivero, T.S. Kaufman, Simultaneous acquisition of the dissolution curves of two active ingredients in a binary pharmaceutical association, employing an on-line circulation system and chemometrics-assistance, J. Pharm. Biomed. Anal. 72 (2013) 51–58.

[55] N.L. Calvo, R.M. Maggio, T.S. Kaufman, An eco-friendly strategy using on-line monitoring and dilution coupled to a second-order chemometric method, for the construction of dissolution curves of combined pharmaceutical associations, J. Pharm. Biomed. Anal. 89 (2014) 213–220.

[56] T. Rajalahti, O.M. Kvalheim, Multivariate data analysis in pharmaceutics: a tutorial review, Int. J. Pharm. 417 (2011) 280–290.

[57] R.B. D'agostino, H.K. Russell, Scree test, Encyclopedia of Biostatistics, Wiley, New York, USA, 2005.

[58] B. Roduit, M. Hartmann, P. Folly, A. Sarbach, R. Baltensperger, Prediction of thermal stability of materials by modified kinetic and model selection approaches based on limited amount of experimental points, Thermochim. Acta 579 (2014) 31–39.

[59] V. Dittrich, W. Topf, O. Kristiansen, *N,N*′-diphenyl-guanidine derivatives, US Patent 4098900, 1978.

[60] A.V. Arbuznikov, L.A. Sheludyakova, E.B. Burgina, Ab initio study of cyanoguanidine isomers, Chem. Phys. Lett. 240 (1995) 239–244.

[61] L. Antonov, Tautomerism: Methods and Theories, Germany, Wiley, Weinheim, 2014.

[62] F.S. de Souza, I.D. Basílio Jr., E.J. Oliveira, R.O. Macêdo, Correlation studies between thermal and dissolution rate constants of cimetidine drug and tablets, J. Therm. Anal. Calorim. 72 (2003) 549–554.